

Article

A Highly Efficient and Durable Kirigami Triboelectric Nanogenerator for Rotational Energy Harvesting

Dae Sol Kong, Jae Yeon Han, Young Joon Ko, Sang Hyeok Park, Minbaek Lee and Jong Hoon Jung * 

Department of Physics, Inha University, Incheon 22212, Korea; lacam062@naver.com (D.S.K.); gkswo0214@gmail.com (J.Y.H.); koyj1006@naver.com (Y.J.K.); sanghayk@naver.com (S.H.P.); mlee@inha.ac.kr (M.L.)

* Correspondence: jhjung@inha.ac.kr; Tel.: +82-32-860-7659

Abstract: While sliding-mode triboelectric nanogenerators (S-TENGs) have been considered as one of the most promising devices for rotational energy harvesting, their inherently poor durability has been a serious bottleneck for applications. Herein, we report a three-dimensional kirigami TENG as a highly efficient and durable rotational energy harvesting device. The kirigami TENG consisted of cube-shaped paper, aluminum (Al) foil electrode and polytetrafluoroethylene (PTFE) polymer film, and converted rotational motion into multiple folding-unfolding vibrations. The rotation-folding (R-F) kirigami TENG generated an open-circuit voltage of 31 V, a short-circuit current of 0.67 μA and an instantaneous power (power density) of 1.2 μW ($0.13 \mu\text{W}/\text{cm}^2$) at 200 rpm, which was sufficient to turn on 25 light-emitting diodes and a thermo-hygrometer. The triboelectric outputs of the R-F kirigami TENG were only slightly decreased even after 288,000 continuous rotations, i.e., the output remained at 86% of its initial value. This work demonstrates that an R-F kirigami TENG could be a plausible candidate to efficiently harvest various forms of rotational energy with a long-term durability.

Keywords: triboelectric nanogenerator; kirigami; rotational energy; durability; efficiency



Citation: Kong, D.S.; Han, J.Y.; Ko, Y.J.; Park, S.H.; Lee, M.; Jung, J.H. A Highly Efficient and Durable Kirigami Triboelectric Nanogenerator for Rotational Energy Harvesting. *Energies* **2021**, *14*, 1120. <https://doi.org/10.3390/en14041120>

Academic Editor:
Abdessattar Abdelkefi

Received: 29 January 2021
Accepted: 17 February 2021
Published: 20 February 2021

Publisher's Note: MDPI stays neutral with regard to jurisdictional claims in published maps and institutional affiliations.



Copyright: © 2021 by the authors. Licensee MDPI, Basel, Switzerland. This article is an open access article distributed under the terms and conditions of the Creative Commons Attribution (CC BY) license (<https://creativecommons.org/licenses/by/4.0/>).

1. Introduction

Mechanical energy harvesting from our daily life has drawn considerable interest due to strong demand for a portable power source to charge numerous mobile devices [1–5]. Among the various mechanical energy harvesting devices, triboelectric nanogenerators (TENGs) have demonstrated the effective conversion of wasted low-frequency vibrations into electricity through a mechanism of triboelectrification and electric induction [6–14]. TENGs have been classified into contact-separation [15,16], single-electrode [17,18], in-plane sliding [19,20] and free-standing modes [21,22], according to their working principles [23]. In particular, sliding mode has been identified as an efficient technique for rotational energy harvesting from the ambient environment.

However, the sliding-mode TENG (S-TENG) has serious drawbacks of energy loss induced by air breakdown and low durability. There have been several important reports to solve or mitigate these deficiencies. Zhou et al. used liquid lubricant to improve power output and durability [24]. They found that liquid lubricant significantly suppressed interfacial breakdown and lowered electrostatic field strength in the micro-gap between the triboelectric layer and electrode. Chen et al. utilized an automatic transitional TENG between contact and non-contact modes [25]. They found that the automatic rotational TENG exhibited less deterioration of output performance. Tang et al. used flexible halbach magnetic array-assisted S-TENG [26]. They found that the magnetic array-assisted S-TENG retained 60% of its initial output after 25 h of continuous operation due to intermittent contact.

In this paper, we report a rotation-folding (R-F) kirigami TENG for rotational energy harvesting with greatly enhanced durability. The R-F kirigami TENG is fabricated from

paper, polyester film, hydrothermally treated aluminum (Al) foil and plasma-treated polytetrafluoroethylene (PTFE) polymer. The unique three-dimensional structure enables the R-F kirigami TENG to transform a single cycle of rotational motion into four folding-unfolding vibrations. Hydrothermal treatment of Al and plasma treatment of PTFE greatly enhances the triboelectric power. We found that such enhancement is related to the increased surface roughness of Al and negative shift of surface potential of PTFE. The R-F kirigami TENG retains 86% of its initial output and clean contacting surface even after 24 h (288,000 cycles) of continuous rotations, in sharp contrast to the 13% of initial output and deteriorated surface in the S-TENG.

2. Experimental Details

2.1. Fabrication

The R-F kirigami TENG was fabricated using normal paper, adhesive tape, polyester film, Al foil and PTFE polymer. Paper (100 μm -thick) was cut into square pieces, attached to polyester film using adhesive tape, and then connected to a cube. Six cubes were assembled together to form a three-dimensional structure. Hydrothermal treatment was performed for as-received Al foils (Sigma Aldrich, Seoul, Korea). The foils were dipped into hot distilled water (ca. 80 $^{\circ}\text{C}$) for 2 h and then cooled in air under flowing N_2 gas. Plasma treatment was performed for as-received PTFE polymers (LK Lab). The polymers were etched at 50 mW for 2 min under flowing Ar gas. Hydrothermally treated Al foils ($3 \times 3 \text{ cm}^2$) were attached to four surfaces of one cube and plasma-treated PTFE polymers ($3 \times 3 \text{ cm}^2$) to one surface of four cubes, as shown in Figure S1.

2.2. Characterization

The surface morphology of Al and PTFE was investigated by atomic force microscopy (XE-7, PSIA, Suwon, Korea) and field-effect scanning electron microscopy (SU 8010, HI-TACHI, Tokyo, Japan). The resistance of Al was measured using an electrometer (6517A, Keithley, Cleveland, OH, USA). The chemical bonding and surface potential of PTFE were investigated by X-ray photoemission spectroscopy with Al $\text{K}\alpha$ radiation (K-Alpha, Thermo Scientific) and Kelvin probe force microscopy (KPFM) (XE-7, PSIA), respectively.

2.3. Triboelectric Power Generation Measurement

A DC motor (DC12V, Motorbank, Seoul, Korea) was used to rotate the R-F kirigami TENG at various angular velocities. Electrical outputs were measured using a digital phosphor oscilloscope (DSOX2002A, Keysight), a programmable electrometer (6517, Keithley, Cleveland, OH, USA) and a low-noise current preamplifier (SR570, Stanford Research Systems, Washington, DC, USA). A bridge rectification circuit and capacitor (1 mF) were used to convert the alternating current into direct current and store the charge, respectively. Light-emitting diodes (LEDs) and thermo-hygrometer were used to demonstrate the powering of small electronic devices.

3. Results and Discussion

To directly show the poor durability of an S-TENG, we performed a control experiment using the same contacting materials of Al and PTFE for an R-F kirigami TENG. Figure 1a shows a schematic illustration and digital images of the S-TENG. Four pieces of Al foils and PTFE films were attached on two acrylic disks at 90° intervals. Then, the two disks were tightly contacted to rotator and stator, and rotated at 200 rpm.

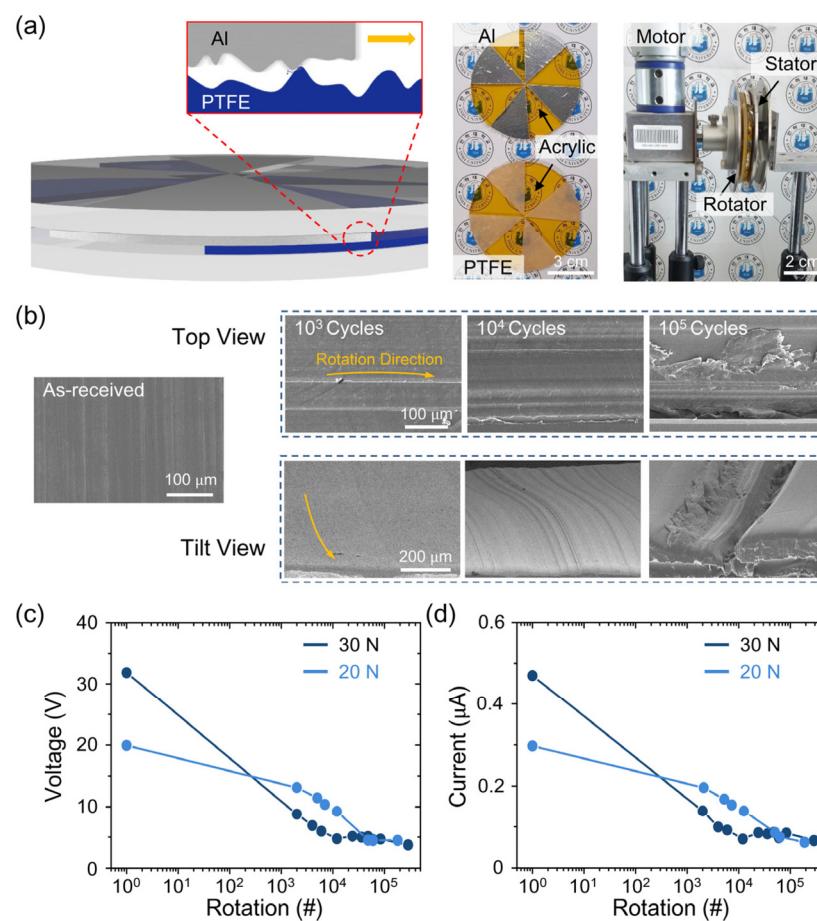


Figure 1. (a) Schematic illustration and optical images of a sliding-mode triboelectric nanogenerator (S-TENG). Rotation number-dependent (b) surface morphology, and (c) open-circuit voltage and (d) short-circuit current. In (b), scanning electron microscopy images of polytetrafluoroethylene (PTFE) are shown for top and tilt views. Orange arrows represent the rotational direction.

Figure 1b shows top and tilt views of PTFE as a function of the number of rotations. There are several lines on the surface of the as-received PTFE. When rotation continues, the PTFE surface becomes scratched along the rotational direction. The scratches are deepened and widened with the increasing number of rotations, reaching a depth of 40 μm and widths of 5–30 μm after 288,000 rotations. A magnified tilt-view clearly shows that the PTFE polymers are seriously damaged after the rotations.

Such deteriorated PTFE surface should significantly decrease triboelectric outputs [27–29]. As shown in Figure 1c,d, respectively, the triboelectric voltage and current sharply decreased and then were nearly saturated after 288,000 rotations. The triboelectric voltage and current retain only 12% and 14% of their initial values, respectively, at 30 N. Triboelectric output should decrease more rapidly with the increase of applied force. It may cause the lowered outputs at large force, as compared with those at small force, after a certain number of rotations. Consistently, the triboelectric output at 30 N is lower than that at 20 N during the rotation number of $2 \times 10^3 \sim 2 \times 10^4$.

To address the poor durability of S-TENGs, we adopted a kirigami approach [30–34]. Figure 2a shows a schematic illustration and digital image of the R-F kirigami TENG. Because of the unique three-dimensional structure, rotation of one cube causes movement of the other cubes in the R-F kirigami TENG [35]. Namely, the rotation of one Al foil-attached cube results in the folding-unfolding vibration of four PTFE polymer-attached cubes. Note that the polyester film takes the role of hinge for the successive folding-unfolding vibration.

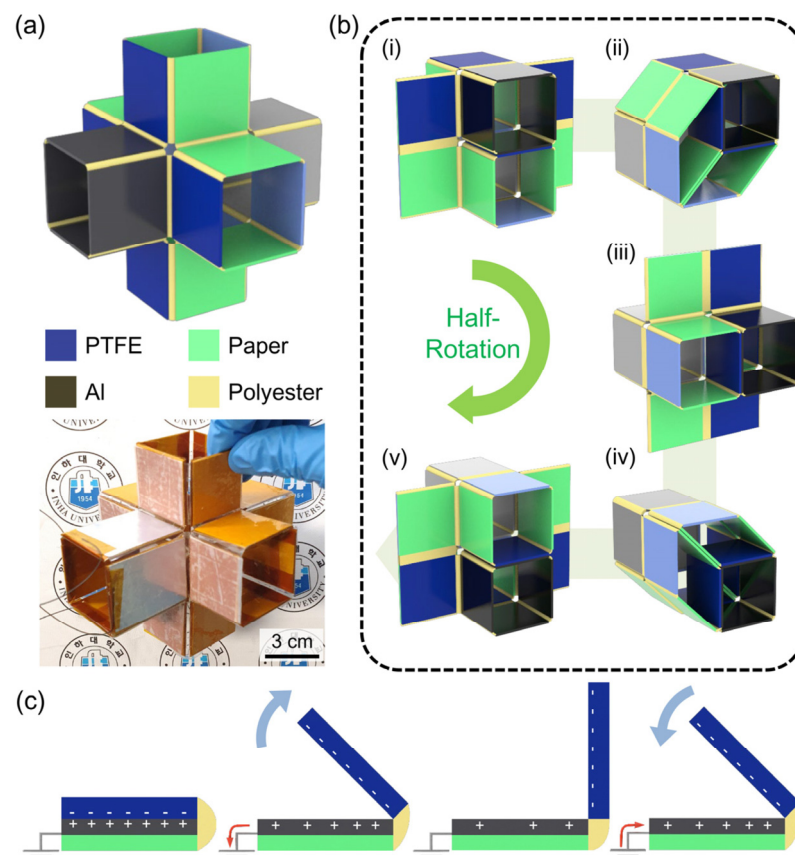


Figure 2. (a) Schematic illustration and digital image of a rotation-folding (R-F) kirigami TENG. (b) Detailed motion of each cube during a half-rotation. (c) Power generation mechanism for a folding-unfolding vibration during a quarter-rotation.

Figure 2b schematically illustrates the detailed movements of each cube during a half-rotation. When an Al-attached cube rotates clockwise by 90° , a left PTFE-attached cube folds while a bottom PTFE-attached cube unfolds. When an Al-attached cube rotates by 180° , a top PTFE-attached cube folds while a left PTFE-attached cube unfolds. Likewise, right and bottom PTFE-attached cubes successively fold, while top and right PTFE-attached cubes successively unfold when an Al-attached cube rotates by 270° to 360° .

In Figure 2c, we schematically illustrate the power generation mechanism of the R-F kirigami TENG for a folding-unfolding vibration during a quarter-rotation. When the PTFE polymer contacts Al foil, the PTFE and Al become negatively and positively charged, respectively, according to the triboelectric series [36]. When the PTFE polymer starts to unfold from the Al foil, a potential difference will be formed, which causes positive charges to flow from the Al foil to the ground until equilibrium. When the PTFE polymer begins to fold again, another potential difference will be formed, which causes positive charges to flow from ground to the Al foil. (Because of folding-unfolding vibration instead of vertical contact-separation, the triboelectric charges in Al foil are not homogeneously distributed to screen the immobile triboelectric charges in PTFE.) Therefore, four current peaks should occur during a one-rotational cycle.

Figure 3a,b show the atomic force microscopy images and resistances, respectively, of as-received and hydrothermally treated Al foils. The hydrothermal treatment significantly increases the roughness of Al foils. Quantitatively, the root-mean-square roughness (R_{rms}) increases from 11.75 to 58.15 nm. On the other hand, the hydrothermal treatment causes little change of resistance from 3.8Ω [37,38]. Increased roughness without changing resistance in Al electrode should assist TENG application through the increased contact area and effective transfer of charge carriers. Figure 3c,d show the X-ray photoemission spectra and surface potential images, respectively, of as-received and plasma-treated PTFE

polymers. The plasma-treatment significantly alters the chemical bonding. Qualitatively, the peak corresponds to C–O bond increases, while that to C–F bond decreases. In addition, the plasma-treatment causes a negative shift of surface potential (V_{rms}) from -14.7 to -29.3 V [39,40]. A negative shift of surface potential in PTFE polymer should also assist TENG application through the transfer of larger amounts of charge carriers. Detailed dimensions and electrical properties of surface-treated Al and PTFE are summarized in Table 1.

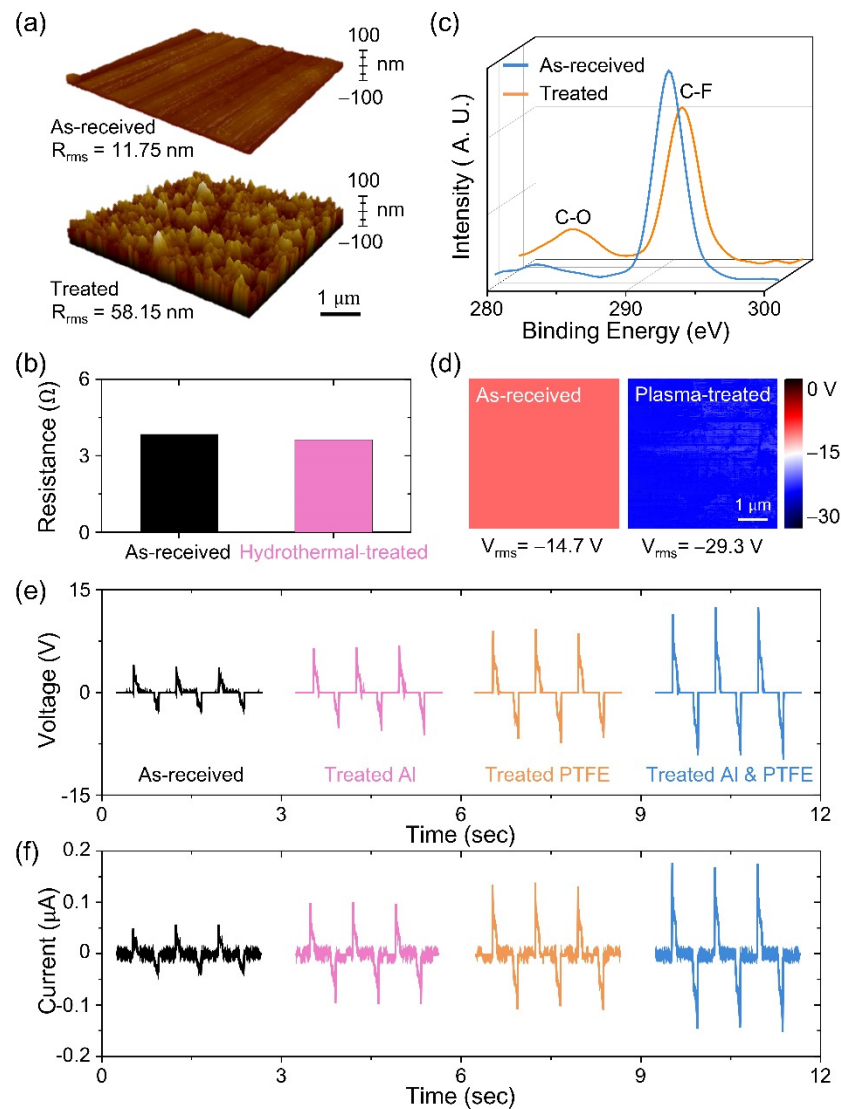


Figure 3. (a) Atomic force microscopy images and (b) resistances of as-received and hydrothermally treated Al foil. (c) X-ray photoemission spectra and (d) surface potentials of as-received and Ar plasma-treated PTFE polymer. Comparison of (e) open-circuit voltage and (f) short-circuit current for various surface treatments.

Table 1. Dimensions and electrical properties of surface-treated Al and PTFE.

	Hydrothermal-Treated Al	Plasma-Treated PTFE
dimension	3×3 cm ²	3×3 cm ²
resistance/resistivity	3.8 Ω	10^{18} Ωm [41]
surface potential	0.8 V [42]	-29.3 V

In Figure 3e,f, we compare the open-circuit voltage and short-circuit current, respectively, of contact separation between Al and PTFE for various surface treatments. The as-received Al and PTFE generate a voltage of 3.7 V and a current of 57 nA, while hydrothermally treated Al and plasma-treated PTFE generate a voltage of 12.5 V and a current of 176.8 nA. Such a remarkable enhancement of triboelectric outputs after the surface treatment in the contact-separation mode should also enhance the triboelectric outputs in the rotational mode.

Using the surface-treated Al and PTFE, we investigate the open-circuit voltage and short-circuit current of an R-F kirigami TENG in Figure 4a,b, respectively, at various rpm. For all angular velocities, many peaks could be observed due to the four folding-unfolding vibrations during one rotation. Overall, the triboelectric outputs increased with increasing angular velocity. Figure 4c shows the external load-dependent voltage, current and power at 200 rpm. Due to Ohm's law, the voltage increases while the current decreases with increasing load resistance. Maximum triboelectric power (power density) of 1.2 μW (0.13 $\mu\text{W}/\text{cm}^2$) is obtained at 100 M Ω .

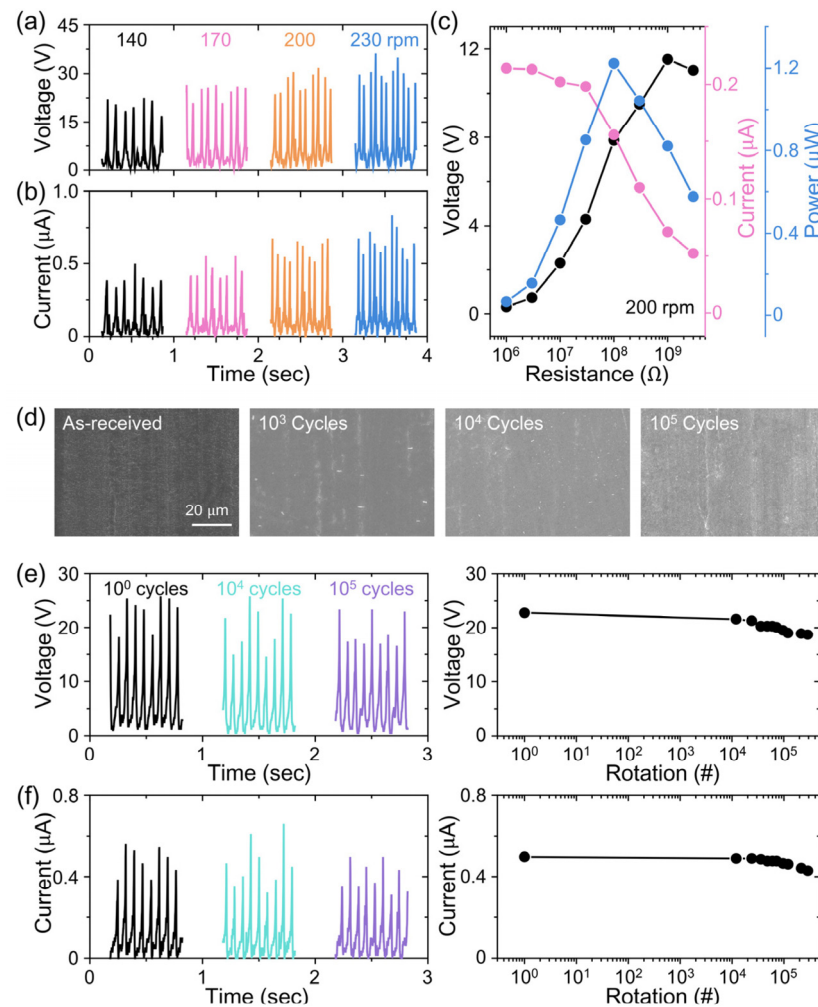


Figure 4. (a) Open-circuit voltage and (b) short-circuit current of an R-F kirigami TENG at various angular velocities. (c) Load resistance-dependent voltage, current and power at 200 rpm. Rotation number-dependent (d) surface morphology of PTFE, and (e) open-circuit voltage and (f) short-circuit current of the R-F kirigami TENG.

The variation of surface morphology and triboelectric outputs of the R-F kirigami TENG are shown in Figure 4d,e,f, respectively. In sharp contrast to the S-TENG (Figure 1), the R-F kirigami TENG retains almost 86% of its initial output even after 288,000 rotations.

Accordingly, the surface morphology of PTFE is almost unchanged, irrespective of the number of rotations. We notice that the choice of an appropriate material for the junction of cubes are crucial for the stability of R-F kirigami TENG. As shown in Figure S2, a weak adhesive tape causes a stability problem, i.e., the R-F kirigami TENG only retains 62% of its initial output, in sharp contrast to a tough polyester film.

An R-F kirigami TENG with greatly enhanced output and durability could be used for the long-term operation of small electronic devices. Figure 5a schematically illustrates the proposed applications of the R-F kirigami TENG for self-powered lightening and self-powered weather monitoring systems in a rural region. The R-F kirigami TENG can convert the rotational motion of a windmill or watermill into electricity via folding-unfolding vibrations. The harvested electricity can be used to operate LEDs, which could help farmers to work in light conditions and operate thermo-hygrometers, which could help them to predict the weather.

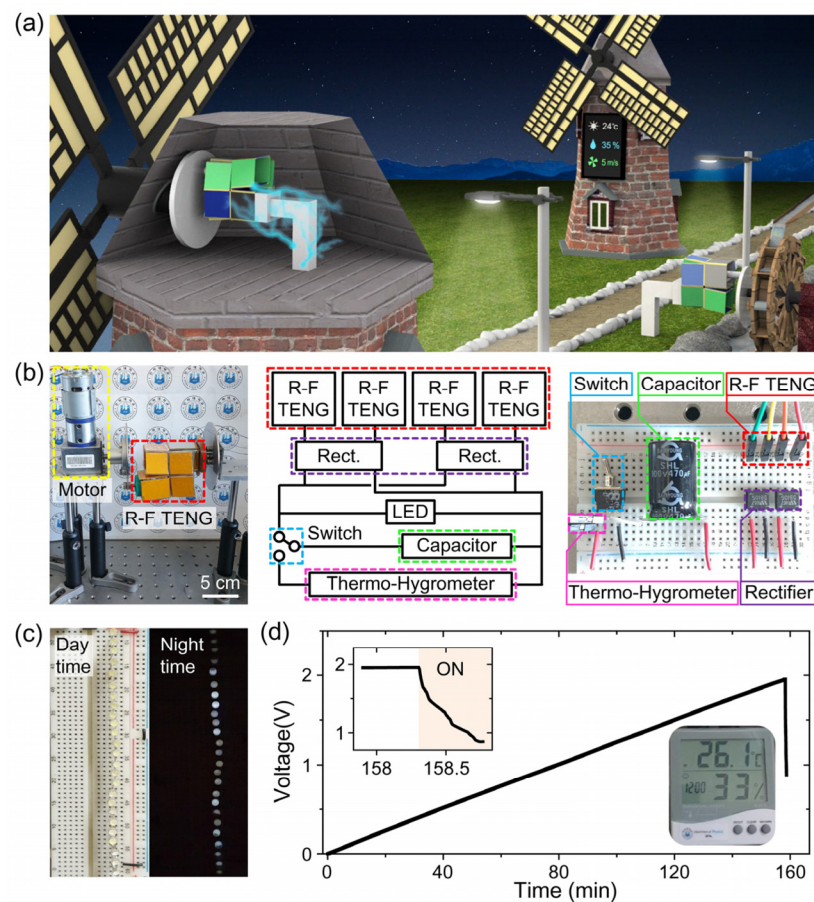


Figure 5. (a) Proposed applications of an R-F kirigami TENG for powering LEDs and a thermo-hygrometer at a windmill and watermill. (b) Circuit diagram and digital photographs of the R-F kirigami TENG, rectifiers, switch, LED and capacitor. (c) Digital photographs of powered LEDs during the day- and night-time. (d) Charging-discharging curve of a 1 mF capacitor. In the inset, detailed discharging curve and powered thermo-hygrometer image are shown.

To demonstrate the feasibility of such applications, we assembled rectifiers, a capacitor, a switch, LEDs and a thermo-hygrometer and connected them to the R-F kirigami TENG (Figure 5b). During the rotation of the R-F kirigami TENG, 25 white LEDs were brightly illuminated during the day- and night-time (Figure 5c, Video S1). During the rotation of the R-F kirigami TENG, the 1 mF capacitor was charged to 2 V within 158 min and operated a thermo-hygrometer for 30 s (Figure 5d, Video S2).

4. Conclusions

In summary, we report a rotation-folding kirigami triboelectric nanogenerator (R-F kirigami TENG) to harvest the wasted rotational energy with greatly enhanced efficiency and durability. The R-F kirigami TENG is fabricated using six cubes made from normal paper, adhesive tape, polyester film, Al foil and PTFE polymer. Three-dimensional R-F kirigami TENG converts a one-rotational cycle into four folding-unfolding vibrations. Hydrothermal and plasma treatments significantly increase the roughness of Al foil and shift the surface potential of PTFE polymer, respectively, thereby greatly improving the triboelectric outputs. The R-F kirigami TENG generates an open-circuit voltage of 31 V, short-circuit current of 0.67 μA and instantaneous power (power density) of 1.2 μW (0.13 $\mu\text{W}/\text{cm}^2$) at 200 rpm. The output power is sufficient to operate 25 LEDs and a thermo-hygrometer. The R-F kirigami TENG retains almost 86% of its initial output even after the 288,000 rotations, in sharp contrast to the 13% in the S-TENG. This work suggests that three-dimensional kirigami-based TENG could be a feasible approach to promote efficiency as well as durability in rotational energy harvesting applications.

Supplementary Materials: The following are available online at <https://www.mdpi.com/1996-1073/14/4/1120/s1>, Figure S1: A fabrication process of an R-F kirigami TENG, Figure S2: Comparison of rotation number dependent normalized open-circuit voltage and short-circuit current when each adhesive tape and polyester film was used at the junction of cubes, Video S1: Powering 25 light-emitting diodes (LEDs) by an R-F kirigami TENG, Video S2: Operation of a thermo-hygrometer by an R-F kirigami TENG.

Author Contributions: Conceptualization, J.H.J. and D.S.K.; investigation and data curation, D.S.K., J.Y.H., Y.J.K., S.H.P. and M.L.; writing—original draft preparation, J.H.J., D.S.K.; writing—review & editing, J.H.J., D.S.K. and M.L. All the authors participated in discussions of the research. All authors have read and agreed to the published version of the manuscript.

Funding: This research was supported by Basic Science Research Program through the National Research Foundation of Korea (NRF) funded by the Ministry of Education, Science and Technology (2020R1A2C1006987 and 2020R1A4A1017915).

Institutional Review Board Statement: Not applicable.

Informed Consent Statement: Not applicable.

Data Availability Statement: Not applicable.

Conflicts of Interest: The authors declare no conflict of interest.

References

1. Wang, Z.L.; Song, J.H. Piezoelectric nanogenerators based on zinc oxide nanowire arrays. *Science* **2006**, *312*, 242–246. [CrossRef]
2. Fan, F.R.; Tian, Q.; Wang, Z.L. Flexible triboelectric generator. *Nano Energy* **2012**, *1*, 328–334. [CrossRef]
3. Wang, Z.L.; Wu, W. Nanotechnology-enabled energy harvesting for self-powered micro-/nanosystems. *Angew. Chem. Int. Ed.* **2012**, *51*, 11700–11721. [CrossRef]
4. Wang, Z.L. Triboelectric nanogenerators as new energy technology for self-powered systems and as active mechanical and chemical sensors. *ACS Nano* **2013**, *7*, 9533–9557. [CrossRef] [PubMed]
5. Jung, J.H.; Lee, M.; Hong, J.-I.; Ding, Y.; Chen, C.-Y.; Chou, L.-J.; Wang, Z.L. Lead-free NaNbO_3 nanowires for a high output piezoelectric nanogenerator. *ACS Nano* **2011**, *5*, 10041–10046. [CrossRef] [PubMed]
6. Chen, J.; Zhu, G.; Yang, W.; Jing, Q.; Bai, P.; Yang, Y.; Hou, T.-C.; Wang, Z.L. Harmonic-resonator-based triboelectric nanogenerator as a sustainable power source and a self-powered active vibration sensor. *Adv. Mater.* **2013**, *25*, 6094–6099. [CrossRef]
7. Chen, J.; Wang, Z.L. Reviving vibration energy harvesting and self-powered sensing by a triboelectric nanogenerator. *Joule* **2017**, *1*, 480–521. [CrossRef]
8. Chen, G.; Li, Y.; Bick, M.; Chen, J. Smart textiles for electricity generation. *Chem. Rev.* **2020**, *120*, 3668–3720. [CrossRef]
9. Hinchet, R.; Yoon, H.-J.; Ryu, H.; Kim, M.-K.; Choi, E.-K.; Kim, D.-S.; Kim, S.-W. Transcutaneous ultrasound energy harvesting using capacitive triboelectric technology. *Science* **2019**, *365*, 491–494. [CrossRef] [PubMed]
10. Yun, B.K.; Kim, H.S.; Ko, Y.J.; Murillo, G.; Jung, J.H. Interdigital electrode based triboelectric nanogenerator for effective energy harvesting from water. *Nano Energy* **2017**, *36*, 233–240.
11. Choi, Y.S.; Jing, Q.; Datta, A.; Boughey, C.; Kar-Narayan, S. A triboelectric generator based on self-poled Nylon-11 nanowires fabricated by gas-flow assisted template wetting. *Energy. Environ. Sci.* **2017**, *10*, 2180–2189. [CrossRef]

12. Wang, Y.; Yang, Y.; Wang, Z.L. Triboelectric nanogenerators as flexible power sources. *Npj. Flex. Electron.* **2017**, *1*, 10. [[CrossRef](#)]
13. Cheng, L.; Xu, Q.; Zheng, Y.; Jia, X.; Qin, Y. A self-improving triboelectric nanogenerator with improved charge density and increased charge accumulation speed. *Nat. Commun.* **2018**, *9*, 3773. [[CrossRef](#)]
14. Chang, T.-H.; Peng, Y.-W.; Chen, C.-H.; Chang, T.-W.; Wu, J.-M.; Hwang, J.-C.; Gan, J.-Y.; Lin, Z.-H. Protein-based contact electrification and its uses for mechanical energy harvesting and humidity detecting. *Nano Energy* **2016**, *21*, 238–246. [[CrossRef](#)]
15. Chen, J.; Huang, Y.; Zhang, N.; Zou, H.; Liu, R.; Tao, C.; Fan, X.; Wang, Z.L. Micro-cable structured textile for simultaneously harvesting solar and mechanical energy. *Nat. Energy* **2016**, *1*, 16138. [[CrossRef](#)]
16. Yang, W.; Chen, J.; Jing, Q.; Yang, J.; Wen, X.; Su, Y.; Zhu, G.; Peng, B.; Wang, Z.L. 3D stack integrated triboelectric nanogenerator for harvesting vibration energy. *Adv. Funct. Mater.* **2014**, *24*, 4090–4096. [[CrossRef](#)]
17. Zou, Y.; Xu, J.; Fang, Y.; Zhao, X.; Zhou, Y.; Chen, J. A hand-driven portable triboelectric nanogenerator using whirligig spinning dynamics. *Nano Energy* **2021**, *83*, 105845. [[CrossRef](#)]
18. Zhu, G.; Chen, J.; Liu, Y.; Bai, P.; Zhou, Y.S.; Jing, Q.; Pan, C.; Wang, Z.L. Linear-grating triboelectric nanogenerator based on sliding electrification. *Nano Lett.* **2013**, *13*, 2282–2289. [[CrossRef](#)]
19. Yang, Y.; Zhang, H.; Chen, J.; Jing, Q.; Zhou, Y.S.; Wen, X.; Wang, Z.L. Single-electrode-based sliding triboelectric nanogenerator for self-powered displacement vector sensor system. *ACS Nano* **2013**, *7*, 7342–7351. [[CrossRef](#)]
20. Zhou, Z.; Chen, K.; Li, X.; Zhang, S.; Wu, Y.; Zhou, Y.; Meng, K.; Sun, C.; He, Q.; Fan, W.; et al. Sign-to-speech translation using machine-learning-assisted stretchable sensor arrays. *Nat. Electron.* **2020**, *3*, 571–578. [[CrossRef](#)]
21. Wang, S.; Xie, Y.; Niu, S.; Lin, L.; Wang, Z.L. Freestanding triboelectric-layer-based nanogenerators for harvesting energy from a moving object or human motion in contact and non-contact modes. *Adv. Mater.* **2014**, *26*, 2818–2824. [[CrossRef](#)]
22. Guo, H.; Chen, J.; Yeh, M.H.; Fan, X.; Wen, Z.; Li, Z.; Hu, C.; Wang, Z.L. An ultrarobust high-performance triboelectric nanogenerator based on charge replenishment. *ACS Nano* **2015**, *9*, 5577–5584. [[CrossRef](#)]
23. Wu, C.; Wang, A.C.; Ding, W.; Guo, H.; Wang, Z.L. Triboelectric nanogenerator: A foundation of the energy for the new era. *Adv. Energy Mater.* **2019**, *9*, 1802906. [[CrossRef](#)]
24. Zhou, L.; Liu, D.; Zhao, Z.; Li, S.; Liu, Y.; Liu, L.; Gao, Y.; Wang, Z.L.; Wang, J. Simultaneously enhancing power density and durability of sliding-mode triboelectric nanogenerator via interface liquid lubrication. *Adv. Energy Mater.* **2020**, *10*, 2002920. [[CrossRef](#)]
25. Chen, J.; Guo, H.; Hu, C.; Wang, Z.L. Robust triboelectric nanogenerator achieved by centrifugal force induced automatic working mode transition. *Adv. Energy Mater.* **2020**, *10*, 2000886. [[CrossRef](#)]
26. Tang, Q.; Pu, X.; Zheng, Q.; Yang, H.; Li, J.; Wu, Y.; Guo, H.; Huang, Z.; Hu, C. A strategy to promote efficiency and durability for sliding energy harvesting by designing alternating magnetic stripe arrays in triboelectric nanogenerator. *Nano Energy* **2019**, *66*, 104087. [[CrossRef](#)]
27. Lin, L.; Xie, Y.; Niu, S.; Wang, S.; Yang, P.-K.; Wang, Z.L. Robust triboelectric nanogenerator based on rolling electrification and electrostatic induction at an instantaneous energy conversion efficiency of ~55%. *ACS Nano* **2015**, *9*, 922–930. [[CrossRef](#)]
28. Seol, M.-L.; Han, J.-W.; Moon, D.-I.; Yoon, K.J.; Hwang, C.S.; Meyyappan, M. All-printed triboelectric nanogenerator. *Nano Energy* **2018**, *44*, 82–88. [[CrossRef](#)]
29. Kim, H.S.; Kim, D.Y.; Kim, J.E.; Kim, J.H.; Kong, D.S.; Murillo, G.; Lee, G.H.; Park, J.Y.; Jung, J.H. Ferroelectric-polymer-enabled contactless electric power generation in triboelectric nanogenerators. *Adv. Funct. Mater.* **2019**, *29*, 1905816. [[CrossRef](#)]
30. Xia, K.; Zhu, Z.; Zhang, H.; Du, C.; Fu, J.; Xu, X. Milk-based triboelectric nanogenerator on paper for harvesting energy from human body motion. *Nano Energy* **2019**, *56*, 400–410. [[CrossRef](#)]
31. Yang, P.-K.; Lin, Z.-H.; Pradel, K.C.; Lin, L.; Li, X.; Wen, X.; He, J.-H.; Wang, Z.L. Paper-based origami triboelectric nanogenerators and self-powered pressure sensors. *ACS Nano* **2015**, *9*, 901–907. [[CrossRef](#)]
32. Kang, Y.; Wang, B.; Dai, S.; Liu, G.; Pu, Y.; Hu, C. Folded elastic strip-based triboelectric nanogenerator for harvesting human motion energy for multiple applications. *ACS Appl. Mater. Interfaces* **2015**, *7*, 20469–20476. [[CrossRef](#)]
33. Wu, C.; Wang, X.; Lin, L.; Guo, H.; Wang, Z.L. Paper-based triboelectric nanogenerators made of stretchable interlocking kirigami patterns. *ACS Nano* **2016**, *10*, 4652–4659. [[CrossRef](#)]
34. Zhang, H.; Yang, C.; Yu, Y.; Zhou, Y.; Quan, L.; Dong, S.; Luo, J. Origami-tessellation-based triboelectric nanogenerator for energy harvesting with application in road pavement. *Nano Energy* **2020**, *78*, 105177. [[CrossRef](#)]
35. Chen, S.; Chen, J.; Zhang, X.; Li, Z.-Y.; Li, J. Kirigami/origami: Unfolding the new regime of advanced 3D microfabrication/nanofabrication with “folding”. *Light Sci. Appl.* **2020**, *9*, 75. [[CrossRef](#)]
36. Diaz, A.F.; Felix-Navarro, R.M. A semi-quantitative tribo-electric series for polymeric materials: The influence of chemical structure and properties. *J. Electrostat.* **2020**, *9*, 75. [[CrossRef](#)]
37. Saifaldeen, Z.S.; Khedir, K.R.; Cansizoglu, M.F.; Demirkan, T.; Karabacak, T. Superamphiphobic aluminum alloy surfaces with micro and nanoscale hierarchical roughness produced by a simple and environmentally friendly technique. *J. Mater. Sci.* **2004**, *62*, 277–290. [[CrossRef](#)]
38. Vedder, W.; Vermilyea, D. A Aluminum + water reaction. *Trans. Faraday Soc.* **1969**, *65*, 561–584. [[CrossRef](#)]
39. Wilson, D.J.; Williams, R.L.; Pond, R.C. Plasma modification of PTFE surfaces. Part I: Surfaces immediately following plasma treatment. *Surf. Interface Anal.* **2001**, *31*, 385–396. [[CrossRef](#)]

-
40. Kim, D.Y.; Kim, H.S.; Kong, D.S.; Choi, M.; Kim, H.B.; Lee, J.-H.; Murillo, G.; Lee, M.; Kim, S.S.; Jung, J.H. Floating buoy-based triboelectric nanogenerator for an effective vibrational energy harvesting from irregular and random water waves in wild sea. *Nano Energy* **2018**, *45*, 247–254. [[CrossRef](#)]
 41. Blythe, A.R. Electrical resistivity measurements of polymer materials. *Polym. Test.* **1984**, *4*, 195–209. [[CrossRef](#)]
 42. Lee, D.W.; Jeong, D.G.; Kim, J.H.; Kim, S.H.; Murillo, G.; Lee, G.-H.; Song, H.-C.; Jung, J.H. Polarization-controlled PVDF-based hybrid nanogenerator for an effective vibrational energy harvesting from human foot. *Nano Energy* **2020**, *76*, 105066. [[CrossRef](#)]